



HAL
open science

^{19}F solid-state NMR approaches to probe antimicrobial peptide interactions with membranes in whole cells

Kiran Kumar, Alexandre Arnold, Raphaël Gauthier, Marius Mamone,
Jean-François Paquin, Dror Warschawski, Isabelle Marcotte

► To cite this version:

Kiran Kumar, Alexandre Arnold, Raphaël Gauthier, Marius Mamone, Jean-François Paquin, et al.. ^{19}F solid-state NMR approaches to probe antimicrobial peptide interactions with membranes in whole cells. *Biochimica et Biophysica Acta: Biomembranes*, 2024, 1866 (3), pp.184269. 10.1016/j.bbamem.2023.184269 . hal-04386127

HAL Id: hal-04386127

<https://hal.science/hal-04386127>

Submitted on 10 Jan 2024

HAL is a multi-disciplinary open access archive for the deposit and dissemination of scientific research documents, whether they are published or not. The documents may come from teaching and research institutions in France or abroad, or from public or private research centers.

L'archive ouverte pluridisciplinaire **HAL**, est destinée au dépôt et à la diffusion de documents scientifiques de niveau recherche, publiés ou non, émanant des établissements d'enseignement et de recherche français ou étrangers, des laboratoires publics ou privés.

1 **¹⁹F solid-state NMR approaches to probe antimicrobial peptide interactions**
2 **with membranes in whole cells**

3 **Kiran Kumar¹, Alexandre A. Arnold¹, Raphaël Gauthier², Marius Mamone²,**
4 **Jean-François Paquin², Dror E. Warschawski^{1,3*} & Isabelle Marcotte^{1*}**

5 ¹Department of Chemistry, Université du Québec à Montréal, P.O. Box 8888, Downtown
6 Station, Montreal, Canada H3C 3P8

7 ²PROTEO, CCVC, Département de chimie, Université Laval, 1045 Avenue de la Médecine,
8 Québec, Québec, G1V 0A6, Canada

9 ³Laboratoire des Biomolécules, LBM, CNRS UMR 7203, Sorbonne Université, École normale
10 supérieure, PSL University, 75005 Paris, France

11 *Corresponding authors

12 Isabelle Marcotte

13 Tel: 1-514-987-3000 #5015

14 Fax: 1-514-987-4054

15 E-mail: marcotte.isabelle@uqam.ca

16
17 Dror E. Warschawski

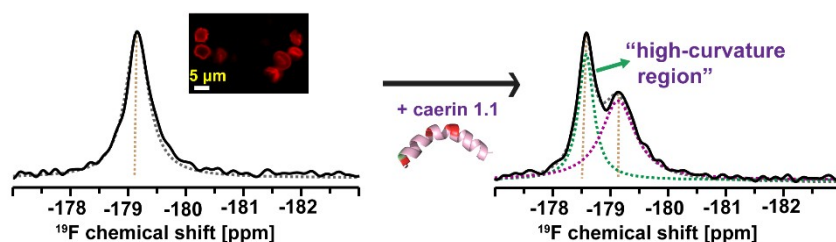
18 Tel : +33 1 44 27 32 16

19 Fax : +33 1 44 27 62 50

20 E-mail: Dror.Warschawski@Sorbonne-Universite.fr

21
22
23
Antimicrobial peptide + erythrocyte ghosts

¹⁹F-ssNMR of intact cells



25 **Abstract**

26 To address the global problem of bacterial antibiotic resistance, antimicrobial peptides (AMPs)
27 are considered promising therapeutic candidates due to their broad-spectrum and membrane-lytic
28 activity. As preferential interactions with bacteria are crucial, it is equally important to
29 investigate and understand their impact on eukaryotic cells. In this study, we employed ^{19}F solid-
30 state nuclear magnetic resonance (ssNMR) as a novel approach to examine the interaction of
31 AMPs with whole red blood cells (RBCs). We used RBC ghosts (devoid of hemoglobin) and
32 developed a protocol to label their lipid membranes with palmitic acid (PA) monofluorinated at
33 carbon positions 4, 8, or 14 on the acyl chain, allowing us to probe different locations in model
34 and intact RBC ghost membranes. Our work revealed that changes in the ^{19}F chemical shift
35 anisotropy, monitored through a C-F bond order parameter (S_{CF}), can provide insights into lipid
36 bilayer dynamics. This information was also obtained using magic-angle spinning (MAS) ^{19}F
37 ssNMR spectra with and without ^1H decoupling, by studying alterations in the second spectral
38 moment (M_2) as well as the ^{19}F isotropic chemical shift, linewidth, T_1 , and T_2 relaxation
39 times. The appearance of an additional isotropic peak with a smaller CSA, a narrower linewidth,
40 and a shorter T_1 , induced by the AMP caerin 1.1, supports the presence of high-curvature regions
41 in RBCs indicative of pore formation, analogous to its antimicrobial mechanism. In summary,
42 the straightforward incorporation of monofluorinated FAs and rapid signal acquisition offer
43 promising avenues for the study of whole cells using ^{19}F ssNMR.

44 **Keywords:** Host defense peptides, red blood cells, lipid bilayer, isotopic labeling, in-cell NMR,
45 model membranes.

46 **Abbreviations:** AMP: antimicrobial peptide; CSA: chemical shift anisotropy; DPPC:
47 dipalmitoylphosphatidylcholine; DPPC- d_{62} : perdeuterated dipalmitoylphosphatidylcholine; GC-
48 MS: gas chromatography coupled to mass spectrometry; L/P: lipid-to-peptide; MAS: magic-
49 angle spinning; MFFA: monofluorinated fatty acid; MLV: multilamellar vesicle; PA: palmitic
50 acid; PA-F(4), (F8) or (F14): palmitic acid fluorinated at positions 4, 8 or 14; S/N: signal-to-
51 noise; ssNMR: solid-state nuclear magnetic resonance; SSB: spinning sideband; T_m : melting
52 temperature.

53 1. Introduction

54 Antimicrobial resistance by disease-causing bacteria has become a global health threat with
55 ensuing socioeconomic issues [1,2]. In recent decades, bacterial resistance has increased at an
56 alarming rate, sustained by an extensive usage of antibiotics. There is thus an urgent need for
57 alternative solutions to combat bacterial resistance and in this context, antimicrobial peptides
58 (AMPs) and their mimics stand as promising antibiotic molecules. Indeed, their action
59 mechanisms involving bacterial membrane disruption, damage to intracellular biomolecules and
60 other oxidative damages [3], are nonspecific and thus hard to evolve against. More than 24,000
61 AMP sequences have been identified so far, both from natural and synthetic origins [4] and only
62 a small number AMPs or their mimics have reached clinical trials [5] or are already
63 commercialized as antimicrobial agents (e.g. bacitracin, gramicidin D, polymyxin B) [5]. *In vivo*
64 stability and low toxicity towards human cells are key factors to access the pharmaceutical
65 market.

66 Since many AMPs target the bacterial lipid membrane, considerable efforts have been put into
67 characterizing their interaction with cell membranes [6,7]. Solid-state NMR (ssNMR) has proved
68 to be a unique tool to study such interactions at a nanoscopic level. Different NMR-active nuclei
69 such as ^1H , ^2H , ^{13}C , and ^{31}P are used to study the biophysical properties of lipid membranes in the
70 presence of AMPs [8-10]. Deuterium is mostly used to characterize lipid chain order and
71 molecular events happening in the core of the bilayer environment, while phosphorus allows
72 probing the lipid headgroups or assessing the overall topology of the lipid organization [11,12].
73 After some initial work on whole cells in the late 70s and early 80s, the field has heavily relied
74 on model membranes until the early 2010s when our group and others reintroduced the use of
75 whole-cell ^2H labelling [13-15]. Our laboratory has also developed the use of magic-angle
76 spinning (MAS) combined to ^2H ssNMR to reduce the experimental time and ensure that cells
77 remain intact [16].

78 ^{19}F is an NMR-active nucleus with interesting properties, notably high sensitivity with low
79 background in biological systems, strong dipolar couplings and a large chemical shift range. This
80 sparked interest in its use to study native membranes already in the late seventies and early eight-
81 ies, with papers showing that the incorporation of fluorinated fatty acid (FA) probes in native
82 membranes was feasible [17,18]. Wild-type and auxotroph *Escherichia coli* strains were success-
83 fully labelled [19,20] as well as *Acholeplasma laidlawii* membranes [17], with FAs fluorinated at

84 different positions, and with only weak perturbations to the membrane [17,19]. McDonough *et*
85 *al.* [18] also showed that monofluorinated palmitic acids (H-C-F) had a less perturbing effect
86 than difluorinated analogues (F-C-F), and also reported that a single fluorine atom in the bilayer
87 was likely to have a less perturbing effect compared to bulkier electron spin or fluorescent
88 probes. In all these studies, it was shown that an order profile along the acyl chains - similar to
89 the one obtained by ^2H ssNMR - could be determined using ^{19}F ssNMR. However, except for one
90 application from the group of Auger [21,22], the use of ^{19}F ssNMR has not been extensively de-
91 veloped to study AMP interactions *from a membrane point of view*. Indeed, the high sensitivity
92 and almost complete absence of this nucleus in nature has stemmed a significant body of work
93 on fluorinated peptides [23-26], but not on fluorinated membranes.

94 Early work on ^{19}F -labelled membranes either by a fluorinated fatty acid or phospholipid fo-
95 cused on static (no magic-angle spinning, MAS) samples and without ^1H decoupling [17-20,27].
96 The order profile in the acyl chains was, however, shown to be accessible and described by order
97 parameters obtained through spectral fitting and normalizing by a rigid linewidth. More recently,
98 ^{19}F -labelled phospholipids synthesis was achieved and these lipids were incorporated into model
99 membranes [22,28-31]. ^{19}F positions spanning the whole acyl chain length and showed by ^{19}F ss-
100 NMR that the ^{19}F chemical shift anisotropy (CSA) decreased monotonically from the headgroup
101 to the end of the acyl chain, thus informing on motion throughout the membrane. They also re-
102 ported the strong ^{19}F isotropic chemical shift variation along the acyl chain. Protons were decou-
103 pled, but MAS was not used in this study.

104 ^{19}F NMR thus appears as an excellent candidate to investigate membrane-AMP interactions in
105 intact cells. In this work, we reintroduce the use of monofluorinated FAs (MFFAs) to label intact
106 red blood cell (RBC) membranes and establish a ^{19}F ssNMR approach to study AMP-membrane
107 interactions. More specifically, we incorporated into erythrocyte ghosts MFFAs labelled at
108 positions 4, 8 and 14 on the acyl chains (**Fig. 1A**). Ghosts are erythrocytes from which
109 hemoglobin has been removed, thus reducing potential interference of the paramagnetic heme
110 group with NMR signals. After an initial assessment on a model membrane, we show how both
111 in-cell static and MAS ^{19}F ssNMR can be exploited to study the pore formation mechanism of
112 AMPs using caerin 1.1 - a natural AMPs isolated from the skin secretions of Australian tree
113 frogs as a model.

114 **2. Materials and methods**

115 **2.1. Materials**

116 Caerin 1.1 was purchased from GenScript Corporation (Piscataway, NJ, USA) with >98 %
117 purity. Protonated and deuterated dipalmitoylphosphatidylcholine (DPPC and DPPC-d₆₂) were
118 obtained from Avanti Polar Lipids (Alabaster, AL, USA). Ethylenediaminetetraacetic free acid
119 (EDTA) was bought from Fisher Scientific (Fair Lawn, NJ, USA), while unlabelled palmitic
120 acid, deuterium-depleted water, Triton X-100, fatty acid methyl ester mix C4-C24 (FAME mix),
121 [16-[(7-nitro-2-1,3-benzoxadiazol-4-yl)amino] palmitic acid (NBD-PA), 1,1'-dilinoylel-3,3',3'-
122 tetramethylindocarbocyanine 4-chlorobenzenesulfonate (Fast DiI) and all other solvents and
123 chemicals were purchased from Sigma Aldrich (Oakville, ON, Canada). Fresh horse RBCs
124 packed 100% were purchased from Cedarlane Laboratories (Burlington, ON, Canada).
125 Deionized 18.2 MΩ.cm Milli-Q water was used in all experiments (Millipore-Sigma, Oakville,
126 ON, Canada). Fluorine-labelled fatty acids were synthesized following a protocol detailed in the
127 SI section.

128 **2.2. Multilamellar vesicles (MLVs) preparation**

129 MLVs were prepared using dry film method as described by Warschawski *et al.* [32]. The
130 lipid mixture (including ¹⁹F-labelled PAs) was dissolved in 1:2 methanol/CHCl₃ solution and
131 dried under nitrogen stream. Remaining traces of organic solvent in the lipid film were removed
132 by high vacuum for at least 2 h. The lipid film was then hydrated with a physiologically-relevant
133 solution of 150 mM NaCl (pH 7.0) prepared with ²H-depleted water. The lipid dispersion was
134 vortexed and freeze-thawed 3 to 5 times (10 min at -20 °C, followed by 10 min above 40-55 °C)
135 and transferred directly into a 4-mm rotor.

136 **2.3. Preparation of ¹⁹F-labelled erythrocyte ghosts**

137 Erythrocyte ghosts were prepared as described by Kumar *et al.* [9]. Briefly, 3-4 mL of
138 concentrated horse RBCs were suspended in a 40 mL round bottom centrifugation tube with 25
139 mL isotonic HEPES buffer (20 mM HEPES, 150 mM NaCl, pH 7.4), and centrifuged at 500 g
140 for 5 min at 4 °C. Then three supplementary washes were done with the same buffer until the
141 supernatant became clear. After the final wash, the pellet was resuspended in 20 mL hypotonic
142 HEPES buffer (20 mM HEPES, pH 7.4) and centrifuged at 25,000 g for 40 min at 4 °C (rotor
143 JA-20, Beckman). The supernatant was then removed, and the pellet transferred into new

144 centrifuge tubes, leaving behind the “red button” that contains proteases. Additional washes (3 to
145 4) with the same buffer were carried out to obtain a hemoglobin-free white ghosts pellet.

146 A mixed micelles solution of 0.5 mM Triton X-100 / 0.25 mM of ¹⁹F-labelled PA in isotonic
147 buffer was prepared in a sealed glass vial with three freeze (-20 °C)/thaw (95 °C)/vortex shaking
148 cycles. The white ghost pellet was then resuspended in 320 mL isotonic buffer to which 80 mL
149 of the mixed micelles solution were transferred, and incubated for 15 min at 37°C. The mixture
150 of ghosts and micellized ¹⁹F-labelled PA was then centrifuged at 25,000 g for 20 min at 4 °C in
151 different 20 mL aliquots. The excess detergent was washed away twice by centrifugation in
152 isotonic buffer at 25,000 g for 20 min at 4 °C. The ghost pellets were pooled together in a 1.5 mL
153 Eppendorf tube and centrifuged at 20,000 g for 20 min at 4 °C. The pellet was then washed with
154 an isotonic buffer and centrifuged at 100,000 g and 4 °C for 20 min. This concentrated pellet was
155 collected and stored at 4°C prior to the experiments and used within 3-4 days.

156 **2.4 Sample preparation for confocal microscopy**

157 A total of 1 % (v/v) of ¹⁹F-labelled ghosts were labelled with the fluorophore Fast-DiI
158 (1/1000) using a 1 h incubation at 37 °C, followed by pelleting at 16,000 g for 15 min, or with
159 NBD-PA directly incorporated into ghosts along with ¹⁹F-labelled PA as described above in
160 section (2.3). The pellet was resuspended in 500 µL of HEPES buffer then transferred to Sarstedt
161 8-well microscopy slides (300 µL) and left to stand for 30 min to allow ghosts immobilization.
162 Samples were incubated for 1 h at 37 °C after addition of an appropriate amount of caerin 1.1
163 into 1 % (v/v) ghosts, and single frame per second images were generated using a Nikon
164 confocal microscope with a 60x oil-immersion lens. Images were processed using ImageJ
165 software.

166 **2.5. Fatty acid profile and labelling efficiency**

167 FA analyses were carried out using gas chromatography coupled to mass spectrometry
168 (GCMS) as described by Laydevant et al. [33] following lipid extraction and transesterification.
169 Briefly, lipids were extracted (triplicates) using the Folch protocol[14], then transesterified using
170 2 mL of H₂SO₄ (2% in methanol) and 0.8 mL of toluene for 10 min at 100 °C. A polar HP-5MS
171 column (30 m length 250 µm diameter 0.25 µm film thickness) was used with an injection
172 volume of 1 µL, and the oven temperature was programmed to heat at 140 °C for 5 min followed

173 by a 4 °C /min ramp up to 300 °C, prior to electron ionization and detection with a Agilent
174 quadrupole MS. Data acquisition and processing were done with the Chemstation software.

175 **2.6. Solid-state NMR and spectral analysis**

176 All ssNMR spectra were recorded using a Bruker Avance III-HD wide-bore 400 MHz
177 spectrometer (Milton, ON, Canada) equipped with a double tuned 4mm-HFX probe and a ¹H-¹⁹F
178 filter. Static ¹⁹F and ³¹P ssNMR spectra were obtained using a phase-cycled Hahn echo pulse
179 sequence, with an inter pulse delay of 35 μs and high-power (50 kHz) ¹H decoupling during
180 acquisition. The 90° pulse length was 4 μs for ¹⁹F ssNMR and 3 μs for ³¹P ssNMR. Data were
181 collected using 2048 points for ¹⁹F ssNMR and 1024 points for ³¹P ssNMR. The recycle delay
182 was 2 s for ¹⁹F ssNMR and 3 s for ³¹P ssNMR. A total of 12 k scans per ¹⁹F spectra for ghosts and
183 1 k scans for MLVs were collected, amounting to 7 hours of acquisition for ghosts and 35 mins
184 for MLVs. And a total of 14 k scans per ³¹P spectra for ghosts and 1 k scans for MLVs were
185 collected, amounting to 12 hours of acquisition for ghosts and 50 mins for MLVs. The ³¹P
186 chemical shifts were referenced to the phosphoric acid (H₃PO₄) signal at 0 ppm, while the ¹⁹F
187 chemical shifts were referenced to the trifluoroacetic acid (TFA) signal at -76.5 ppm.

188 ²H and ¹⁹F ssNMR experiments were also carried out at 10 kHz MAS frequency. A phase-
189 cycled Hahn echo sequence was used for both MAS ²H ssNMR experiments with MLVs samples
190 and MAS ¹⁹F ssNMR analysis of ghosts. ²H ssNMR spectra were recorded with 100 k data
191 points, a 4 μs 90° pulse length, rotor-synchronized interpulse delay of 96 μs and recycle time of
192 500 ms. A total of 1024 scans per spectra were collected, amounting to 8 min acquisition time.
193 ¹⁹F ssMAS spectra were collected with 3 k data points, a 4 μs 90° pulse length, rotor-
194 synchronized interpulse delay of 94 μs and recycle time of 2 s. In model membrane sample a
195 total of 512 scans per spectra were collected, amounting to 18 minutes of acquisition time with a
196 recycle time of 2 s and in ghost sample a total of 6k scans per spectra were collected, amounting
197 to 3.5 hours of acquisition time with a recycle time of 2 s.

198 ³¹P and ¹⁹F CSA values were determined by line fitting using the Bruker Topspin 4.0.6
199 software with Sola (Solid Lineshape Analysis) program and values from minimum two replicates
200 are reported. Since the CSA is proportional to the order parameter, a bond order parameter S_{CF}
201 was calculated using equation (1)[19]. The ¹⁹F CSA measured on pure and dry fluorinated PAs at
202 -30 °C was taken as the rigid CSA (≈ 18 ppm):

203
$$S_{CF} = \frac{\text{Observed } ^{19}\text{F CSA}}{\text{Rigid } ^{19}\text{F CSA}} \quad (\text{Equation 1})$$

204 ^2H spectral moment analysis was performed using MestRenova software V6.0 (Mestrelab
 205 Research, Santiago de Compostela, Spain). Second spectral moments, M_2 , were calculated using
 206 equation (2) [34,35] and values from minimum two replicates are reported.

207
$$M_2 = \omega_r^2 \frac{\sum_{N=0}^{\infty} N^2 A_N}{\sum_{N=0}^{\infty} A_N} = \frac{9 \Pi^2 \square_Q^2}{20} \langle S_{CD}^2 \rangle \quad (\text{Equation 2})$$

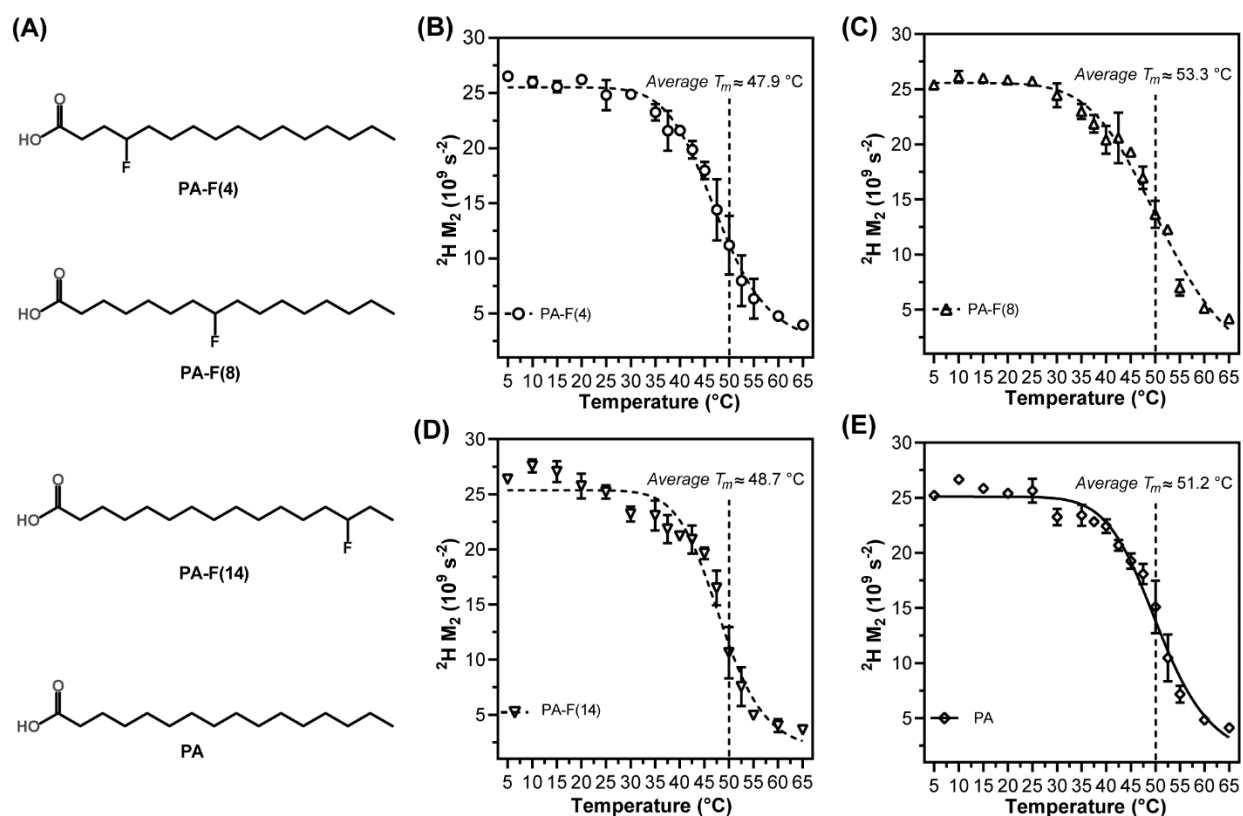
208 where ω_r is the angular spinning frequency, N is the side band number, and A_N is the area of each
 209 sideband obtained by spectral integration, S_{CD}^2 is the mean square order parameter, and \square_Q is the
 210 static quadrupolar coupling constant equal to 168 kHz for a C-D bond in acyl chains. The M_2
 211 value provides a quantitative description of the membrane lipid ordering and is particularly
 212 sensitive to the gel-to-fluid phase transition. In the case of ^{19}F ssNMR, M_2 can also be
 213 determined using the first part of equation 2.

214 **3. Results**

215 **3.1. Fluorinated FAs as reporters of membrane structure and order**

216 FAs are molecular probes that can be readily incorporated into biological membranes to study
 217 their biophysical properties in native cellular conditions [9]. The incorporation of exogenous FAs
 218 into living cells is often easier than other labelling strategies exploiting the cell's biochemistry
 219 [36,37]. Moreover, free FAs are natural constituents of cell membranes where they are involved
 220 in various cellular processes and play a role in regulating cellular functions and membrane
 221 fluidity [38]. However, incorporating high concentrations of FAs can change the bilayer phase
 222 behavior - an effect that has been addressed in previous works [39-42]. For example, the gel
 223 (L_β)-to-fluid (L_α) phase transition temperature (T_m) of a lipid membrane is increased by the
 224 presence of FAs, and a coexistence of gel and fluid phases can occur at certain phospholipid/FA
 225 ratios [41]. Nevertheless, FAs remain accurate reporters of variations in the lipid order in a
 226 membrane system [41]. Therefore, before incorporating MFFAs in whole cells' membranes, we
 227 characterized their effect on the membrane fluidity and as a function of the fluorine atom
 228 position on the acyl chain.

229 We used model dipalmitoylphosphatidylcholine (DPPC) membranes to assess the effect of
 230 palmitic acid (PA) fluorinated at positions 4, 8 or 14, referred to as PA-F(4), PA-F(8) and PA-
 231 F(14) (**Fig. 1A**). The addition of perdeuterated DPPC (DPPC-d₆₂) allowed monitoring the
 232 membrane order profile by measuring the variation of the second spectral moment (M_2)
 233 calculated from ²H ssNMR spectra as a function of temperature, as described elsewhere [16,43].
 234 Examples of such spectra, can be found in **Fig. S1**.



236 **Figure 1:** Effect of fluorination on DPPC-d₆₂/PA model membranes. (A) PAs were fluorinated at
 237 different positions along the acyl chain. Second spectral moment (M_2) as a function of
 238 temperature. M_2 values were obtained from the ²H ssNMR MAS spectra (Fig. S1) of
 239 DPPC/DPPC-d₆₂/PA at a molar ratio of (1:1:1) with fluorinated and non-fluorinated PA
 240 analogues, (B) with PA-F(4), (C) PA-F(8), (D) PA-F(14) and (E) PA. M_2 reports on acyl chain
 241 order and values are indicated with standard deviations.

242 The DPPC/PA mixture results in a complex phase diagram in which, at intermediate
 243 temperatures, PA-rich gel and DPPC-rich fluid phases coexist [42]. As shown in **Fig. 1B to 1E**,
 244 the order profile as well as T_m of DPPC varies very little when comparing fluorinated and non-
 245 fluorinated samples. The average T_m determined by ²H ssNMR is centered at ≈ 48 - 53°C . Our
 246 results are consistent with previous studies of the phase behavior of PA-containing DPPC

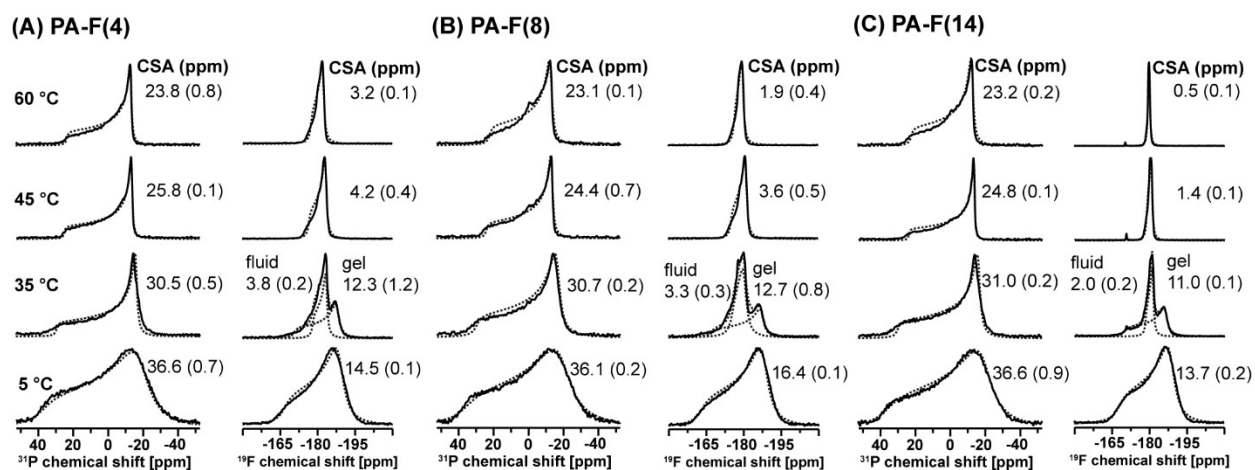
247 bilayers [39,42]. In their investigation of the pseudo-binary phase diagram of DPPC/PA
248 mixtures, Inoue *et al.* [42] reported a $T_m \sim 53\text{-}54^\circ\text{C}$ at 2:1 DPPC/PA molar ratio. The melting of
249 the acyl chain can also be monitored using the ^1H ssNMR intensity of the main-chain CH_2 peak,
250 as well as other lipid resonances (**Fig. S2**). In this case, T_m is centered at $\sim 53\text{-}54^\circ\text{C}$ (**Fig. S3**) - a
251 difference expected between protonated and deuterated phospholipid analogues [44]. Overall,
252 our results show that the insertion of one fluorine atom in the bilayer (positions 4, 8 and 14 on
253 PA acyl chain), has a very weak perturbing effect.

254 The pioneering work on ^{19}F -labelled biological membranes from the late 70's and early 80's
255 was technically limited to non-spinning samples and ^{19}F detection without ^1H decoupling. The
256 single recent work on membranes labelled with monofluorinated phospholipids carried out by
257 Gagnon *et al.* [22] showed that, with ^1H decoupling, the ^{19}F lineshape could be used to assess the
258 local order at a given acyl chain position. They also reported a strong ^{19}F isotropic chemical shift
259 difference along the phospholipid acyl chains - a property that could be exploited to determine
260 the acyl chain order in multiply labelled FAs or lipids using MAS. In their study, similarities are
261 observable between ^{31}P and ^{19}F lineshapes, indicating that ^{19}F could be exploited in a similar
262 fashion to ^{31}P to study the formation of fast tumbling structures that can be induced by
263 membrane-active AMPs [45]. This is notably the case of AMPs that act through a carpet
264 mechanism [9,45].

265 We verified whether ^{19}F ssNMR spectra of model membranes labelled with MFFAs could
266 reflect changes in membrane structure and acyl-chain local order. **Fig. 2** compares the static ^{31}P
267 and ^{19}F ssNMR spectra of DPPC membranes incorporating PA-F(4), PA-F(8) or PA-F(14). ^{31}P
268 spectra indicate changes in the phospholipids headgroup dynamics while ^{19}F spectra probe the
269 hydrophobic region of the bilayer. The ^{31}P spectra lineshapes in **Fig. 2** are characteristic of lipids
270 in a lamellar phase with axial symmetry, and clearly reveal a gel (L_β)-to-fluid (L_α) phase
271 transition. For such systems, this transition can be quantified by measuring the chemical shift
272 anisotropy (CSA), which value is related to the spectrum width and decreases with increasing
273 molecular dynamics. As seen in **Fig. 3A**, characteristic gel phases were detected up to 30°C with
274 a ^{31}P CSA value of 36 ppm that gradually dropped to 25 ppm at 45°C , as the first components of
275 the bilayer reach their phase transition temperature. In comparison, we determined CSA of 36-40
276 ppm in pure DPPC/DPPC- d_{62} membranes (**Fig. S4**) at a gel phase (up to 25°C), which gradually

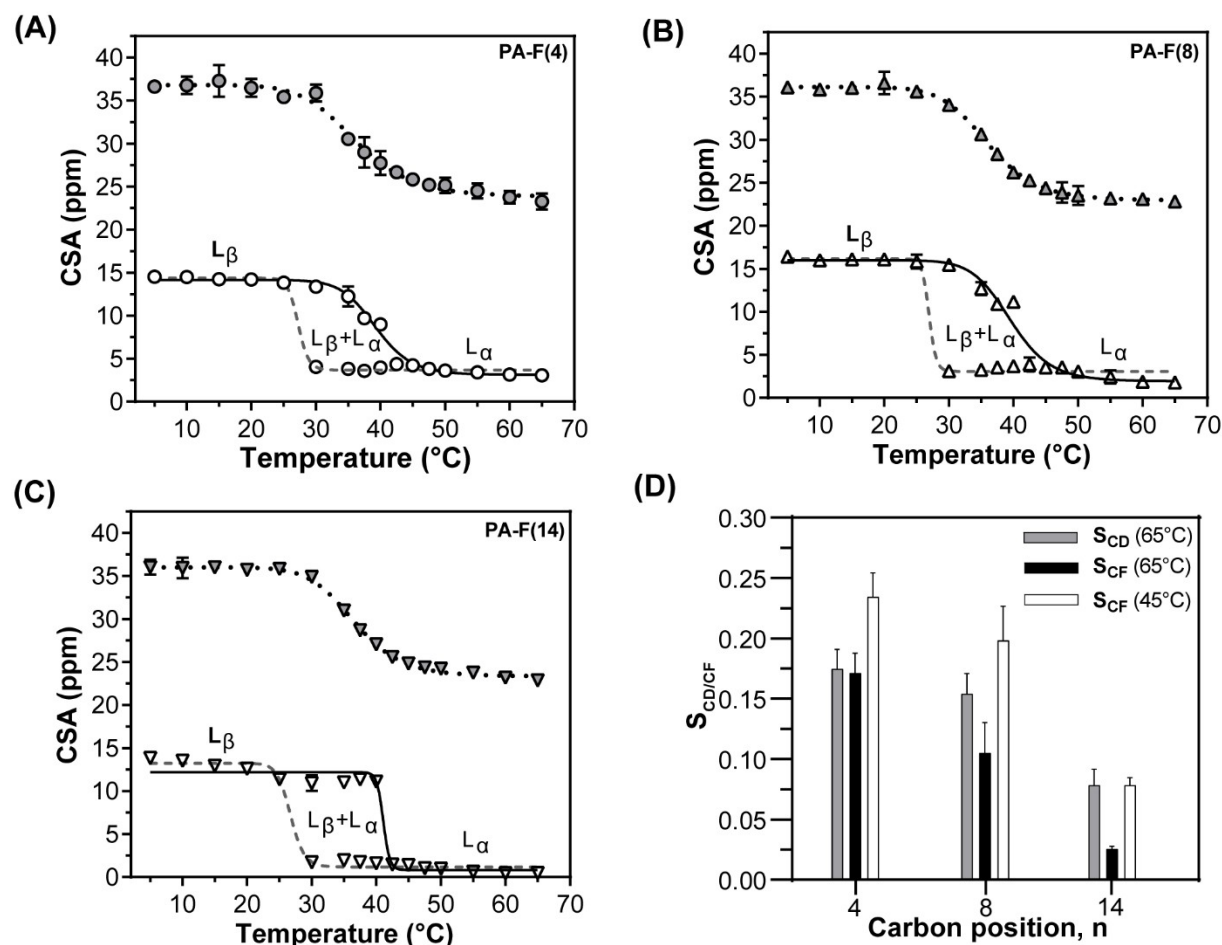
277 dropped to 29 ppm at the fluid phase (42 °C). The addition of protonated PA shifted T_m to ~45-
 278 50 °C, as expected from the DPPC-PA phase diagram [42].

279 ^{19}F ssNMR lineshapes of the MFFAs show strong similarities with ^{31}P ssNMR spectra, in
 280 particular in the gel phase with powder patterns characteristic of multilamellar vesicles (**Fig. 2**).
 281 As shown in **Fig. 3A**, the change in CSA values through the gel-to-fluid phase transition is
 282 analogous to the one observed with ^{31}P ssNMR. The gel phase is maintained up to 25 °C with ^{19}F
 283 CSA values of 14-16.5 ppm, and a noticeable larger CSA of 16.5 ppm when the ^{19}F -label is on
 284 the 8th carbon position, indicating a higher degree of order at the center of the lipid monolayer.
 285 Although ^{19}F CSA values are smaller than those of ^{31}P , they are very sensitive to changes in
 286 membrane fluidity. Indeed, when transitioning from the gel to the fluid phase, ^{19}F CSA values
 287 are reduced by 87% on average. Above 25 °C up to about 42 °C, a coexistence of gel and fluid
 288 phases is observed in the ^{19}F spectra (**Fig. 2 and 3A-C**), consistent with the DPPC-PA phase
 289 diagram [42]. In the fluid phase, the ^{19}F CSA values range from ~1 ppm (PA-F(14)) to 4 ppm
 290 (PA-F(4)), depending on the fluorine atom position. This result is in agreement with the
 291 conformation and order profile along the acyl chains, with position 4 close to the headgroup
 292 undergoing less *trans-gauche* isomerisations than the 14th position, closer to the terminal methyl
 293 group.



295 **Figure 2:** Static ^{31}P and ^{19}F ssNMR spectra of DPPC model membranes incorporating
 296 monofluorinated PAs, at a DPPC/DPPC- d_{62} /PA molar ratio of 1:1:1. (A) with PA-F(4), (B) PA-
 297 F(8) and (C) PA-F(14). Experiments were performed at different temperatures with ^1H
 298 decoupling. Fitted spectra are shown as dashed lines. Average CSA values are indicated, with
 299 standard deviation.

300 Positioning ^{19}F atoms at different places along the FA acyl chain enables assessing the local
 301 order of the bilayer's hydrophobic region, from the interface to the core [19,22,27]. Providing
 302 that FAs undergo fast rotational motion along their long axis, this order can be quantified by
 303 introducing an order parameter, which describes the dynamic reorientation of a bond with respect
 304 to the main axis. This parameter is obtained by normalizing a given NMR-measured quantity in a
 305 mobile segment by its value in the static case. In the case of ^2H ssNMR for example, this is the
 306 quadrupolar coupling for a static C-D bond [43].



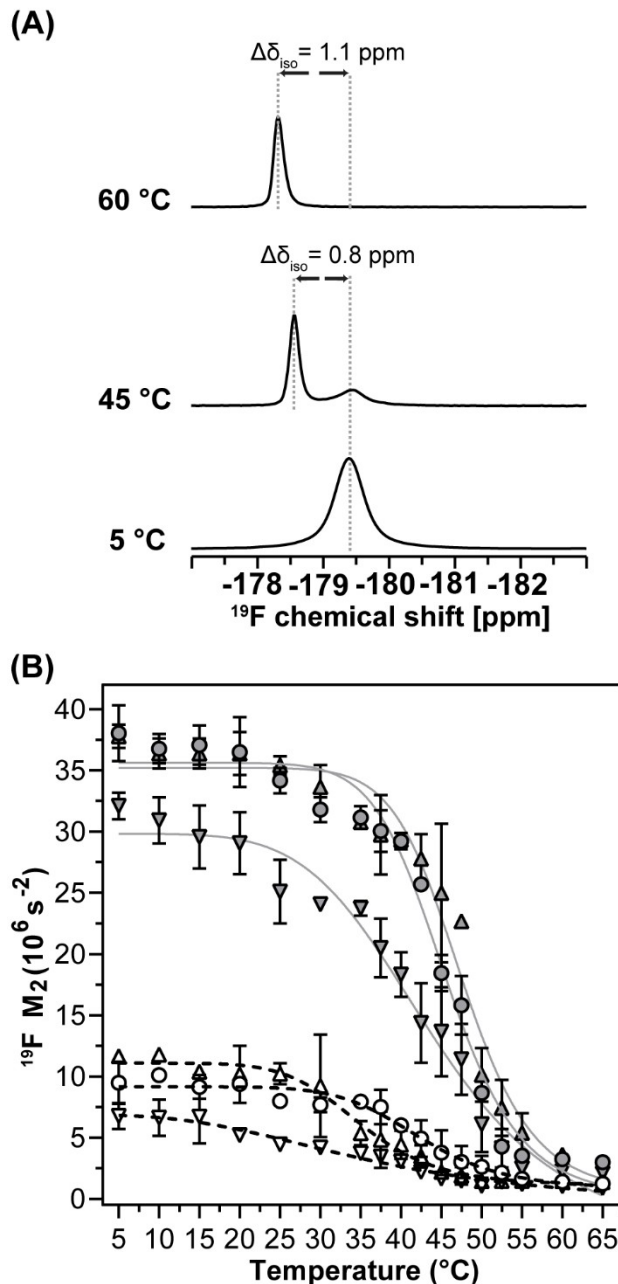
308 **Figure 3:** Temperature dependence of the static ^{31}P (dotted lines) and ^{19}F (solid and dashed lines)
 309 CSA values for DPPC membranes with monofluorinated PAs at a molar ratio of 1:1, calculated
 310 from Fig. 2. (A) PA-F(4), (B) PA-F(8) and (C) PA-F(14) with filled symbols corresponding to
 311 ^{31}P ssNMR and empty ones to ^{19}F ssNMR. Note the presence of two components detected by ^{19}F
 312 ssNMR in the coexistence region. (D) ^2H (S_{CD}) and ^{19}F (S_{CF}) order parameter profile of the acyl
 313 chain in ^{19}F -labelled DPPC membranes as a function of the fluorine atom position, at 45 and 65
 314 °C, with standard deviation.

315 In early ^{19}F ssNMR studies, spectra were recorded without ^1H decoupling; the CSA and
316 dipolar couplings interactions could therefore not be isolated, and were estimated by computer-
317 assisted line fitting [19,27]. When employing high-power ^1H decoupling, it is reasonable to
318 assume that only the CSA persists, simplifying the determination of the order parameter [46].
319 Here, we introduced a C-F bond order parameter, S_{CF} , defined as the ratio between the
320 experimentally-measured CSA and its value for an immobile C-F bond (Equation 1). By
321 definition a rigid molecule with an all-*trans* conformation has an order parameter of $S_{\text{CF}} = 1$
322 while this value is 0 in the case of fast isotropic motions. The ^{19}F CSA tensor is not aligned along
323 the C-F bond, and not necessarily axially symmetric, but in the fluid phase it becomes pseudo-
324 axially symmetric with respect to the FA's long axis, as reflected in the spectra. **Fig. 3D** shows
325 the S_{CF} bond order parameters for PA-F(4), -F(8) and -F(14) in model membranes. As a means of
326 comparison, the S_{CD} order parameter of DPPC- d_{62} measured in the same sample is also presented
327 (**Fig. S5**). The similarity of S_{CF} and S_{CD} values suggests that the relative orientation of the ^{19}F
328 CSA tensor with respect to the molecular frame is factored out when the dry FA at -30°C is used
329 as the reference spectrum. The evolution of the two order parameters adequately reflect dynamic
330 changes with carbon position and temperature, confirming that the S_{CF} of MFFAs can be
331 efficiently employed to measure the order profile along the acyl chains.

332 In the case of intact cells, measuring the acyl chain order at each carbon position is usually
333 impossible. When perdeuterated lipids are used, the distribution of quadrupolar couplings, which
334 reflects the overall dynamics in the membrane, can be assessed by measuring the second spectral
335 moment, M_2 , of the ^2H ssNMR spectra [43]. As we showed in a previous work, M_2 can also be
336 determined under MAS conditions, which enhances the signal-to-noise (S/N) ratio and decreases
337 the acquisition time [16]. **Fig. 4** shows ^{19}F ssNMR spectra obtained in the gel and fluid states
338 under 10 kHz MAS. The resulting increase in S/N ratio with respect to the static spectra is *ca.* \approx
339 5-6-fold, corresponding to a reduction in acquisition time by a factor 25-36 for the same S/N
340 ratio. This substantial gain in sensitivity enables recording spectra without ^1H decoupling (**Fig.**
341 **S6**) - an important alternative considering that not all laboratories are equipped with probes
342 capable of detecting ^{19}F while decoupling ^1H . Additionally, it allows working with significantly
343 lower proportions of FAs in the membrane, as demonstrated in Fig. S7. At an MAS frequency of
344 10 kHz, the ^{19}F CSA (ranging between 0.3 kHz in the fluid phase and 6.5 kHz in the gel phase)
345 should be entirely averaged out. Note that the CSA varies linearly with the static magnetic field

346 strength, necessitating faster spin rates at higher fields. While spectra are dominated by an
347 isotropic peak (δ_{iso}), 1-2 spinning sidebands (SSBs) are observed even in the ^1H -decoupled
348 spectra albeit with lower intensity as compared to non-decoupled spectra. In principle, ^1H - ^{19}F
349 dipolar couplings should be eliminated by the strong ^1H decoupling, and the intermolecular ^{19}F -
350 ^{19}F dipole-dipole interactions significantly reduced by MAS. However, it is possible that residual
351 dipolar couplings (^1H - ^{19}F and/or ^{19}F - ^{19}F) remain, or that internal acyl chain motions result in
352 incomplete MAS averaging. In both cases, a change in membrane fluidity would lead to a
353 corresponding alteration in the SSBs' intensities – as is indeed observed when temperature is
354 varied. This feature can be exploited to assess the overall membrane dynamics, as will be shown
355 below. It would be interesting to record the spectra at different magnetic fields in order to
356 determine the relative contribution of field-dependent interactions, such as CSA, to the spinning
357 sideband intensities.

358 The isotropic chemical shift (**Table S1**) is sensitive to the ^{19}F position on the FA chain, and
359 also to the membrane lipid phase for positions 8 and 14 (**Fig. 4 and Fig. S6**). Indeed, two peaks
360 are observed in the gel-fluid coexistence region (between 25 °C and 52 °C) separated by up to
361 0.8 ppm for these positions. The isotropic resonances are separated by up to 1.1 ppm between the
362 gel (5 °C) and fluid (60 °C) phases (**Fig. 4A**). These peaks are easier to distinguish in the ^1H -
363 decoupled spectra where they are almost baseline-resolved. As mentioned, the presence of SSBs
364 allows measuring the ^{19}F spectral moment value (M_2), which reports on the membrane fluidity.
365 **Fig. 4B** shows the evolution of M_2 as a function of temperature for both ^1H -coupled and
366 decoupled spectra. Spinning sidebands were more intense when no decoupling was applied and
367 the M_2 values varied between $38 \times 10^6 \text{ s}^{-2}$ in the gel phase down to $2\text{-}3 \times 10^6 \text{ s}^{-2}$ at 60 °C (fluid
368 phase) for ^{19}F at positions 4 and 8. When the 14th carbon was ^{19}F -labelled (closer to the terminal
369 methyl group) the M_2 value was smaller in the gel phase ($25\text{-}32 \times 10^6 \text{ s}^{-2}$) as compared to PA-F(4)
370 and PA-(F8), but their M_2 values in the fluid phase were all very similar ($2\text{-}3 \times 10^6 \text{ s}^{-2}$). When ^1H
371 decoupling was applied, the SSBs' intensity was significantly reduced, as previously mentioned.
372 The M_2 values dropped to 6.8 and $11.7 \times 10^6 \text{ s}^{-2}$ in the gel phase for positions 8 and 14,
373 respectively. In the fluid phase, the SSBs almost disappeared and the M_2 values were further
374 reduced to $1 \times 10^6 \text{ s}^{-2}$. Overall, our results show that M_2 values vary sufficiently between the gel
375 and fluid phases for both ^1H -coupled and decoupled spectra to be used to assess membrane
376 fluidity and detect phase transition temperatures. When feasible, we recommend recording the



377 spectra with and without ^1H decoupling. In favorable cases, ^1H decoupling might allow
 378 determining the gel phase proportion by a simple integration of the isotropic lines since the ^{19}F
 379 isotropic chemical shift varies with membrane melting. On the other hand, the second spectral
 380 moment variation is larger on spectra without ^1H decoupling and membrane fluidity can thus be
 381 assessed from the M_2 with a higher precision.

382

383 **Figure 4:** **(A)** MAS (10 kHz) ^{19}F ssNMR spectra of DPPC/PA-F(8) model membranes, with
 384 change in isotropic chemical shift ($\Delta\delta_{\text{iso}}$) values as function of temperature. **(B)** Second spectral

385 moment with standard deviation, calculated from the ^{19}F ssNMR MAS spectra (Fig. S6) of
386 DPPC/DPPC- d_{62} with fluorinated PAs analogues in a 1:1:1 molar ratio. Experiments were carried
387 out at different temperatures with (black, dashed line) and without (grey, solid line) ^1H
388 decoupling and symbols are (○): PA-F(4), (△): PA-F(8) and (▽): PA-F(14).

389

390 Since MAS considerably enhances the signal intensity, we further evaluated the membrane
391 dynamics in a site-resolved fashion by measuring the spin-lattice (T_1) and spin-spin relaxation
392 (T_2) times at each position by ^{19}F ssNMR (**Table S1**). Both T_1 and T_2 values increased as the ^{19}F
393 atom position moved from the headgroup region to the center of the bilayer. The same trend was
394 observed with increasing temperature (data not shown), confirming that T_1 and T_2 values indeed
395 report changes in dynamics. The concomitant increase in T_1 with dynamics indicate that the
396 correlation times of the motions contributing to longitudinal relaxation are in the nanosecond
397 timescale, i.e. faster than the inverse of the Larmor frequency ($\tau_c < 1/\omega_0 \approx 3$ ns). Motions with
398 this type of correlation times are most likely trans-gauche isomerisations. If such motions are
399 affected by the interaction with AMPs, a corresponding change in T_1 should thus be observed.

400 3.2. Monofluorinated fatty acids to study whole cell membranes

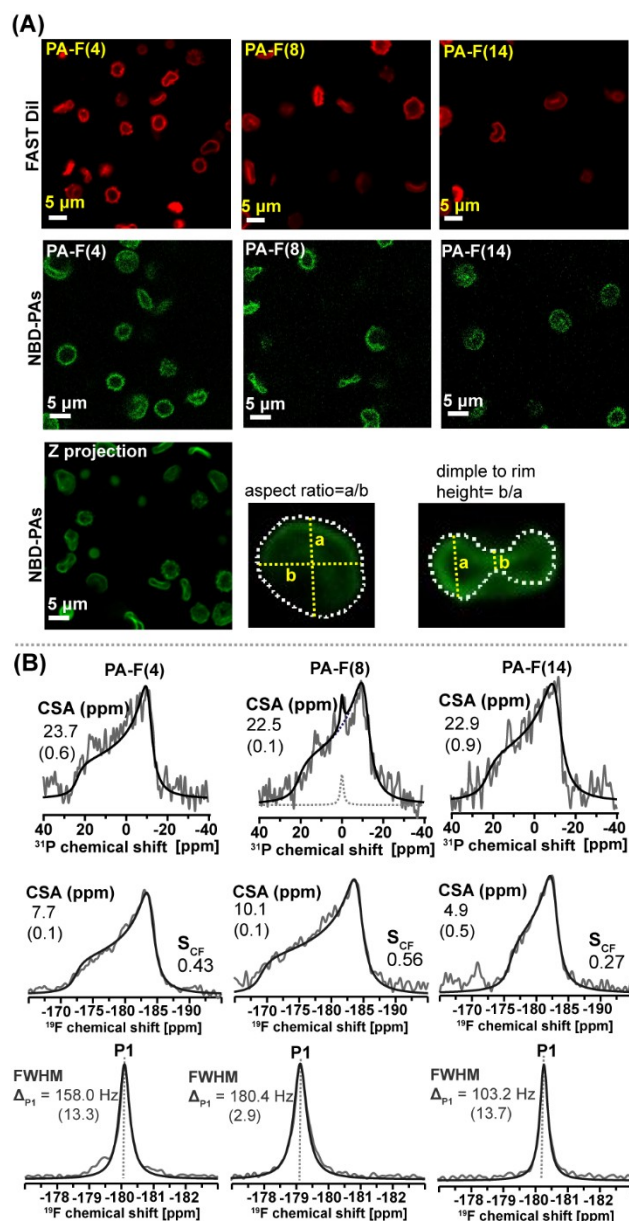
401 Once the ^{19}F ssNMR methods were established in model membranes, we assessed their
402 application to study membranes in intact cells. Early work on bacterial membranes established
403 the possibility of labelling intact bacteria with fluorinated FAs [19,27]. Here, we focused on
404 erythrocyte ghosts, which we had successfully labelled with deuterated PA (PA- d_{31}) in a previous
405 study [9]. Using a similar protocol, we achieved the incorporation of MFFAs into ghosts with
406 labelling levels up to 30%, as determined by GC-MS (**Fig. S8**). Moreover, fluorescence
407 microscopy images of the ^{19}F -labelled ghosts obtained with the lipophilic tracer FAST-DiI and
408 the NBD-PA fluorophore, which is structurally similar to PA, show that they retain their original
409 RBC morphology (**Fig. 5A**).

410 **Fig. 5B** shows static ^{19}F ssNMR spectra of RBC ghosts incorporating MFFAs at 20 °C, which
411 are all characteristic of lipids in a lamellar phase. ^{31}P ssNMR spectra are also shown for
412 comparison. Note that all the different phospholipid headgroups in ghosts, which contain ca.
413 43% PC, 23% phosphatidylethanolamine, 6% phosphatidylserine and 22% sphingomyelin,
414 contribute to the broad ^{31}P NMR spectra [9]. As was the case in model membranes, ^{19}F spectra
415 are characteristic of the acyl chain order at each carbon position. Indeed, the ^{19}F CSA value at the

416 4th position close to PA's headgroup is 7.7 ppm, which is smaller than at the 8th position (10.1
417 ppm). The small CSA value of 4.5 ppm at position 14 reflects the high mobility in the middle of
418 the bilayer. As established in section 3.1, we used the CSA values to determine the order
419 parameter as a function of the fluorine atom position, and found S_{CF} values of 0.43, 0.56 and 0.27
420 for positions 4, 8 and 14, respectively. the higher order determined for PA-F(8) is in line with the
421 characteristics expected in a membrane with a high cholesterol content, where the central portion
422 of the acyl chains is known to be more rigid compared to the chain's beginning or end [47].

423 ¹⁹F ssNMR MAS spectra (**Fig. 5B**) show that the trend of the isotropic linewidth as a function
424 of the fluorine atom position is similar to that of the CSA values. The more rigid 8th position has
425 the broadest full width at half maximum (FWHM=180 Hz), followed by the 4th position (158 Hz)
426 then the more mobile 14th position (103 Hz). We further explored the membrane dynamics by
427 monitoring the ¹⁹F relaxation times of the MFFAs' isotropic resonance in ghosts (which we will
428 refer to as P₁ peak). As reported in Table 1, T₁ values vary with the ¹⁹F atom position, similarly to
429 model DPPC membranes. Values of 328, 414 and 607 ms were respectively determined for
430 positions 4, 8 and 14, i.e., shorter than in DPPC bilayers. This suggests that fluorinated PA
431 probes experience an increase in motions on the nanosecond timescale when incorporated in the
432 ghost membranes, revealing the higher fluidity of ghost membranes as compared to those formed
433 by DPPC. T₂ values in ghosts, which range from 1.5 ms for F(4) to 2.4 ms for F(14), do not differ
434 significantly from those determined in model membranes, implying that millisecond timescale
435 motions are similar in these two types of bilayers. The T₂ value for PA-F(8) is the lowest (1.3
436 ms), consistent with the lowest FWHM value.

437 The isotropic peaks observed on ¹⁹F ssNMR MAS spectra are sufficiently well separated to be
438 resolved in a mixture of the three FAs, or if a triply labelled FA was prepared. The acyl chain
439 order could then be studied in a single experiment while benefiting from the high sensitivity
440 offered by MAS, providing that a triple labelling would not affect the membrane assembly.
441 Altogether, our results show that both the membrane structure and dynamics are measurable by
442 labelling whole cells such as RBC ghosts with MFPA. Their physicochemical properties can
443 thus be investigated, enabling the study of their interaction with membrane-active molecules.



445

446 **Figure 5: (A)** Confocal fluorescence microscopy images of erythrocyte ghosts labelled with
 447 monofluorinated PAs. Secondary fluorophore labelling was achieved using lipophilic tracer
 448 FAST DiI (red) after fluorination, NBD-PA (green) labelling was achieved along with the
 449 fluorination protocol. Scale bars are 5 μm and Z projection image of labelled ghosts with an
 450 average aspect ratio is indicated **(B)** Static ^{31}P (top), static ^{19}F (middle) and ^{19}F MAS (10 kHz)
 451 ssNMR spectra of erythrocyte ghosts labelled with monofluorinated PAs, recorded at 293 K with
 452 ^1H decoupling. CSA and FWHM values are indicated, with standard deviation. Note the
 453 significant improvement in S/N ratio between ^{31}P and ^{19}F NMR.

454

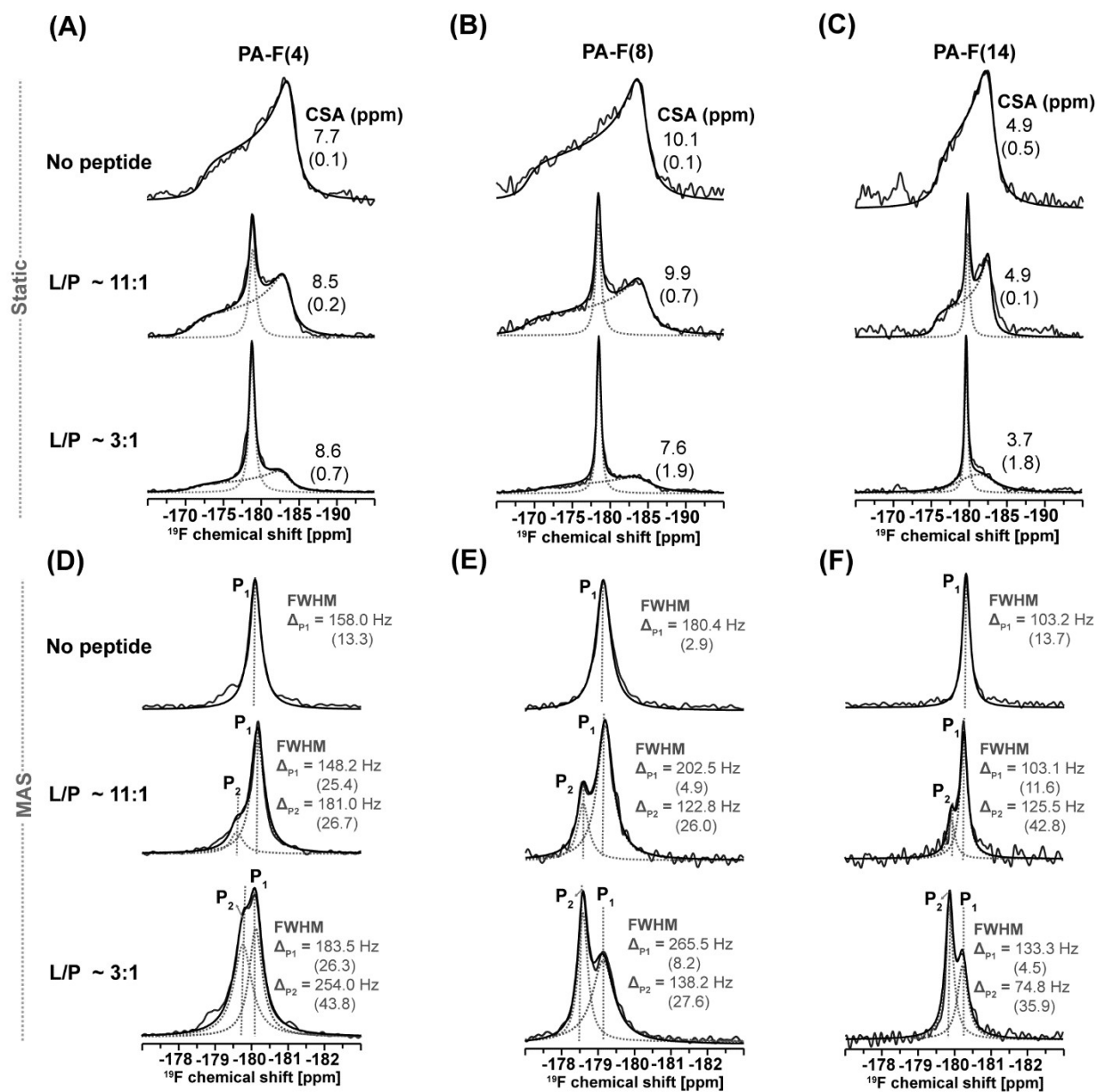
455 3.3. Interaction of caerin 1.1 with ¹⁹F-labelled erythrocyte ghosts

456 We verified the applicability of our ¹⁹F ssNMR approach to study the interaction mechanism
457 of an AMP with intact cells. To do so, we used caerin 1.1 – a 25 amino-acid cationic peptide
458 with the following primary sequence: GLLSVLGSVAKHVLPVVPVIAEHL-NH₂. This AMP
459 was shown to create pores in RBC ghosts labelled with deuterated PA (PA-d₃₁) by ³¹P and ²H
460 ssNMR in our previous work [9]. **Fig. 6A-C** present the static ¹⁹F ssNMR spectra of the ghosts
461 labelled at positions 4, 8 and 14, for different lipid-to-peptide (L/P) molar ratios. The ³¹P ssNMR
462 spectra are available in the SI (**Fig. S9**) for comparison. The ¹⁹F spectra show the presence of a
463 central resonance at approximately 180 ppm with a linewidth ranging from 300 to 400 Hz in the
464 presence of caerin 1.1. Rather than resulting from small fast tumbling objects, the breadth of this
465 line could for example indicate the presence of high-curvature regions in the ghost membranes
466 (see below). ¹⁹F CSA values decrease as a function of peptide concentration for ghosts containing
467 PA-F(8) and PA-F(14), indicating an increased mobility at these positions. An opposite trend is
468 observed for ghosts labelled with PA-F(4), suggesting a proximity of the AMP to the headgroup
469 region of the membrane with local motion hindrance.

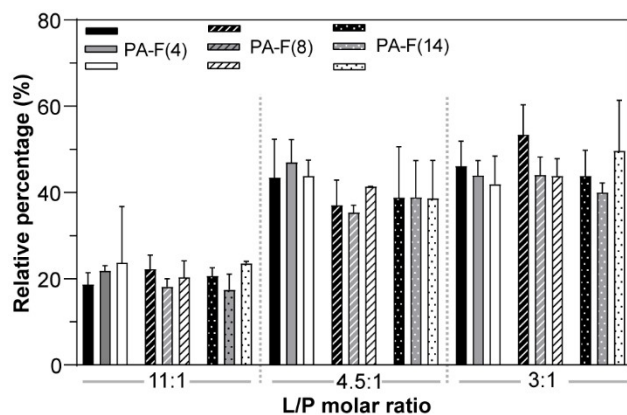
470 The membrane perturbing effect revealed by ¹⁹F static NMR (and ³¹P) correlates well with
471 caerin-induced RBC leakage assays [9]. Indeed, the appearance of the isotropic peak in the
472 ghosts and the RBC leakage occur at roughly the same L/P ratios. These observations are in good
473 agreement with our previous work [9] as well as fluorescence microscopy images in **Fig. S10**,
474 which suggest the formation of pores in the ¹⁹F-labelled ghosts membrane. It should be noted that
475 the L/P ratio refers to the total number of molecules present *in the whole sample*; the local ratio
476 at the actual membrane is most certainly smaller due to AMP partitioning between the membrane
477 and buffer.

478 **Fig. 6D-F** show the ¹⁹F MAS ssNMR spectra of fluorinated ghosts with different
479 concentrations of caerin 1.1. As was the case in model membranes, the anisotropic interactions
480 are conveniently averaged by MAS even at a moderate frequency of 10 kHz. Without peptide,
481 the area of each broad spectrum is concentrated into a single narrow line (noted P₁) with an
482 associated increase in the S/N ratio. Interestingly, when caerin is added, an additional resonance
483 (P₂) emerges and its intensity increases with peptide concentration. This peak is observed with all
484 MFFA analogues. Both P₁ and P₂ resonances are best resolved when the ¹⁹F atom is located at
485 positions 8 and 14. The appearance of two isotropic peaks upon caerin addition suggests that the

486 MFFAs are in two different environments, which we quantified by integrating P₁ and P₂ lines. As
 487 shown in **Fig. 7 (Table S2)**, the P₂ contribution to the MAS ¹⁹F ssNMR spectra is in excellent
 488 agreement with the isotropic contribution to the static ¹⁹F and ³¹P ssNMR spectra.
 489



491 **Figure 6:** Static (A-C) and MAS (D-F) ¹⁹F ssNMR spectra of erythrocyte ghosts labelled with
 492 PA-F(4) (A and D), PA-F(8) (B and E) and PA-F(14) (C and F), exposed to different
 493 concentrations of caerin 1.1. Spectra were recorded at 293 K with ¹H decoupling. CSA and
 494 FWHM values are indicated, with standard deviation. Note the changes of linewidth with
 495 fluorine position.



497 **Figure 7:** Isotropic contribution in the static ^{31}P (black) and ^{19}F (grey) ssNMR spectra compared
 498 to the P_2 contribution (white) in the MAS (10 kHz) ^{19}F ssNMR spectra as a function of caerin 1.1
 499 concentration in erythrocyte ghosts containing monofluorinated PAs.

500 We then explored dynamics changes in the membrane in the presence of AMPs by measuring
 501 T_1 and T_2 relaxation times under MAS. At all fluorine atom positions, the T_1 relaxation time of
 502 the P_2 resonance is consistently shorter than that of P_1 by approximately 100 ms, suggesting that
 503 the presence of interacting caerin increases the motions on the nanosecond timescale that
 504 contribute to T_1 relaxation. On the other hand, the T_2 values are similar for P_1 and P_2 . When
 505 comparing the T_1 and T_2 values of the ghosts/AMP systems with those of MFFAs incorporated in
 506 fast reorienting isotropic dodecylphosphocholine (DPC) micelles, Table 1 shows that P_2 's T_1
 507 values are slightly lower, and T_2 values are an order of magnitude smaller in the AMP-perturbed
 508 ghosts.

509 The presence of an isotropic peak in the static spectra, a small change in T_1 and strong
 510 reduction in T_2 have been shown, in the case of ^{31}P ssNMR, to be characteristic of high-curvature
 511 regions such as cubic or hexagonal phases [48,49]. In full analogy, we thus assign the isotropic
 512 peak in our static ^{19}F spectra and P_2 peak in the MAS spectra to high-curvature regions induced
 513 by the AMP. Our NMR and microscopy results rule out a carpet mechanism, which leads to the
 514 formation of micelles. *A contrario*, the presence of high curvature regions could be due to the
 515 formation of toroidal pores for example, a result consistent with our leakage assay and
 516 fluorescence microscopy results [9]. Control experiments (not shown) rule out the possibility of
 517 hexagonal phase formation.

518

519

520 **Table 1:** Average ^{19}F chemical shifts and ^{19}F T_1 values in different systems incorporating
 521 monofluorinated PA probes, with standard deviation. Values calculated from MAS ^{19}F ssNMR
 522 spectra recorded at 293 K with ^1H decoupling.

^{19}F analogue	DPC Micelles			DPPC/DPPC- d_{62} /PA			Ghosts* (P_1)			Ghosts + Caerin 1.1 (P_2)		
	δ_{iso} (ppm)	T_1 (ms)	T_2 (ms)	δ_{iso} (ppm)	T_1 (ms)	T_2 (ms)	δ_{iso} (ppm)	T_1 (ms)	T_2 (ms)	δ_{iso} (ppm)	T_1 (ms)	T_2 (ms)
PA-F(4)	-180.4	382 (53)	23.8 (14.6)	-180.9	611 (47)	1.7 (0.2)	-180.1	328 (27)	1.5 (0.3)	-179.7	226 (24)	1.1 (0.1)
PA-F(8)	-178.2	487 (18)	18.4 (8.1)	-179.7	760 (163)	2.2 (0.1)	-179.2	414 (4.2)	1.3 (0.4)	-178.6	310 (77)	0.9 (0.1)
PA-F(14)	-179.9	731 (10)	24.9 (5.8)	-181.3	883 (54)	2.2 (0.1)	-180.3	607 (19.1)	2.4 (0.1)	-179.9	472 (69)	1.8 (0.2)

523 * P_1 has the same isotropic chemical shift and T_1 values, without and with caerin 1.1.

524 4. Discussion

525 The objective of this study was to leverage the labelling of whole cells with MFFAs to
 526 investigate specific interactions using ^{19}F ssNMR. Fluorine offers several key advantages,
 527 including high sensitivity, which reduces acquisition time (a critical factor for whole-cell and *in*
 528 *vivo* studies), low occurrence in biological samples, which minimizes background signals, and a
 529 broad chemical shift range, allowing for sensitivity to even minor structural changes. Fluorine is
 530 an isostere of hydrogen that alters the hydrogen bonding properties and dipole moment of the
 531 molecule in which it is incorporated [50,51]. As a consequence, fluorination can change the
 532 polarity and hydrophobicity of a molecule to an extent that will depend on the location and level
 533 of fluorination [50]. Here, we showed, as have others in similar systems, that the incorporation of
 534 MFFAs has only minor effects on the membrane structure [19,22,27], and that it can report
 535 changes in the bilayer's dynamics that are of great relevance to the study of membrane-protein
 536 interactions [19,27,33,52]

537 Using model DPPC membranes incorporating PA fluorinated at three different positions along
 538 the acyl chains, we established that changes in the ^{19}F CSA, isotropic chemical shift and
 539 linewidth, as well as T_1 and T_2 relaxation times, can inform on changes in the lipid bilayer
 540 dynamics. To further characterize these changes, we introduced the order parameter S_{CF} as well
 541 as M_2 measurements, similar to the widely used ^2H ssNMR study of perdeuterated lipids. We
 542 then showed that ^{19}F ssNMR is a valuable tool to describe the membrane state in whole
 543 erythrocyte ghosts and to monitor AMP-membrane interactions. The results obtained here using

544 our ^{19}F ssNMR methodology are consistent with previous work reporting a pore formation
545 mechanism for caerin, thus validating our approach.

546 ^{19}F static spectra enabled the distinction between lamellar and non-lamellar phases with a
547 higher sensitivity than ^{31}P ssNMR. Preliminary data also show that hexagonal phases can be
548 identified by ^{19}F ssNMR (data not shown). In addition, ^{19}F ssNMR with appropriate labelling
549 could replace ^{31}P ssNMR in membranes deprived of phospholipids, such as plant membranes for
550 example. The spectra can be interpreted in terms of an order parameter reflecting the acyl chain
551 order in a similar way to static ^2H ssNMR. The use of MAS, combined to the large chemical shift
552 range of ^{19}F NMR enables distinguishing lamellar and high-curvature regions in a spectrum
553 where anisotropic interactions are fully averaged and all the intensity is concentrated into sharp
554 peaks. This greatly reduces the experimental time and also opens the possibility of measuring
555 relaxation times, allowing to probe dynamical properties of the molecules.

556 In summary, by adequately selecting the ^{19}F position on the acyl chain, ^{19}F ssNMR can
557 provide the same information as ^2H and ^{31}P ssNMR in lipid systems. Typically, knowledge of
558 acyl chain order necessitates the measurement of anisotropic interactions such as CSA,
559 quadrupolar couplings, or dipolar couplings [32,35]. While the simplest approach may involve
560 studying static samples, it is conceivable to reintroduce these anisotropic interactions, thereby
561 harnessing the advantages offered by both MAS and static spectra [32]. In this regard, the
562 broader range of ^{19}F chemical shifts, compared to ^{31}P and even more so to ^2H , becomes
563 advantageous. Additionally, information obtained from anisotropic interactions can be readily
564 complemented by relaxation time measurements, as demonstrated in this study.

565 **5. Conclusions**

566 In this work, we showed how ^{19}F ssNMR is a useful tool to understand the interaction of
567 AMPs with model membranes and, more importantly, whole cells. The incorporation of
568 fluorinated FA probes placed at different depths in the membrane enables mapping changes in
569 dynamics at various locations in the membrane hydrophobic core, thus complementing other
570 biophysical methods such as ^{31}P ssNMR to describe membrane-peptide interactions. Considering
571 its location in the middle of the acyl chain, PA-F(8) would be the preferred MFFA if a single
572 position needs to be chosen. ^{19}F ssNMR experiments can be carried out with static samples or
573 under MAS, with and without ^1H decoupling, each of these approaches having its advantages.

574 The results presented in this work should guide the choice of a ^{19}F ssNMR experiment to
575 investigate lipid membranes in both model and cell systems, whether it concerns membrane
576 structure, dynamics, or a peptide mode of action. We exemplified our methodology with the
577 study of the cationic AMP caerin 1.1 as it interacts with erythrocyte membranes. The labelling
578 strategy presented in this work should be widely applicable to other cells such as bacteria.

579 **6. Acknowledgements**

580 This research was funded by the Natural Sciences and Engineering Research Council
581 (NSERC) of Canada (grant RGPIN-2018-06200 to I.M.) and the Centre National de la
582 Recherche Scientifique (UMR 7203 to D.E.W.). K.K. would like to thank the Quebec Network
583 for Research on Protein Function, Engineering, and Applications (PROTEO) - strategic cluster of
584 the Fonds de recherche du Québec – Nature et technologies (FRQNT) - for the award of a
585 scholarship. The authors thank Dr. Mathew Sebastiao (Université du Québec à Montréal) for
586 technical assistance and Pierre Audet (Université Laval) for the loan of the HFX probe.

587 **7. References**

- 588 [1] M.I. Hutchings, A.W. Truman, B. Wilkinson, Antibiotics: past, present and future, *Current*
589 *opinion in microbiology*, 51 (2019) 72-80.
- 590 [2] S.B. Levy, The challenge of antibiotic resistance, *Scientific American*, 278 (1998) 46-53.
- 591 [3] M. Magana, M. Pushpanathan, A.L. Santos, L. Leanse, M. Fernandez, A. Ioannidis, M.A.
592 Giulianotti, Y. Apidianakis, S. Bradfute, A.L. Ferguson, The value of antimicrobial peptides in
593 the age of resistance, *The Lancet Infectious Diseases*, 20 (2020) e216-e230.
- 594 [4] U. Gawde, S. Chakraborty, F.H. Wagh, R.S. Barai, A. Khandekar, R. Indraguru, T. Shirsat,
595 S. Idicula-Thomas, CAMPR4: a database of natural and synthetic antimicrobial peptides, *Nucleic*
596 *Acids Res*, 51 (2023) D377-D383.
- 597 [5] K. Browne, S. Chakraborty, R. Chen, M.D. Willcox, D.S. Black, W.R. Walsh, N. Kumar, A
598 new era of antibiotics: the clinical potential of antimicrobial peptides, *International journal of*
599 *molecular sciences*, 21 (2020) 7047.
- 600 [6] C. Aisenbrey, A. Marquette, B. Bechinger, The mechanisms of action of cationic
601 antimicrobial peptides refined by novel concepts from biophysical investigations, *Antimicrobial*
602 *Peptides: Basics for Clinical Application*, (2019) 33-64.

603 [7] N. Harmouche, B. Bechinger, Lipid-mediated interactions between the antimicrobial peptides
604 magainin 2 and PGLa in bilayers, *Biophysical journal*, 115 (2018) 1033-1044.

605 [8] E. Strandberg, A.S. Ulrich, NMR methods for studying membrane-active antimicrobial
606 peptides, *Concepts in Magnetic Resonance Part A: An Educational Journal*, 23 (2004) 89-120.

607 [9] K. Kumar, M. Sebastiao, A.A. Arnold, S. Bourgault, D.E. Warschawski, I. Marcotte, In situ
608 solid-state NMR study of antimicrobial peptide interactions with erythrocyte membranes,
609 *Biophysical Journal*, 121 (2022) 1512-1524.

610 [10] A. Naito, N. Matsumori, A. Ramamoorthy, Dynamic membrane interactions of antibacterial
611 and antifungal biomolecules, and amyloid peptides, revealed by solid-state NMR spectroscopy,
612 *Biochimica et Biophysica Acta (BBA)-General Subjects*, 1862 (2018) 307-323.

613 [11] M. Meier, J. Seelig, Lipid and peptide dynamics in membranes upon insertion of n-alkyl- β -
614 D-glucopyranosides, *Biophysical journal*, 98 (2010) 1529-1538.

615 [12] I. Marcotte, M. Auger, Bicelles as model membranes for solid-and solution-state NMR
616 studies of membrane peptides and proteins, *Concepts in Magnetic Resonance Part A: An
617 Educational Journal*, 24 (2005) 17-37.

618 [13] J. Pius, M.R. Morrow, V. Booth, ^2H solid-state nuclear magnetic resonance investigation of
619 whole *Escherichia coli* interacting with antimicrobial peptide MSI-78, *Biochemistry*, 51 (2012)
620 118-125.

621 [14] C. Tardy-Laporte, A.A. Arnold, B. Genard, R. Gastineau, M. Morancais, J.-L. Mouget, R.
622 Tremblay, I. Marcotte, A ^2H solid-state NMR study of the effect of antimicrobial agents on intact
623 *Escherichia coli* without mutating, *Biochimica et Biophysica Acta (BBA)-Biomembranes*, 1828
624 (2013) 614-622.

625 [15] X.L. Warnet, A.A. Arnold, I. Marcotte, D.E. Warschawski, In-cell solid-state NMR: an
626 emerging technique for the study of biological membranes, *Biophysical journal*, 109 (2015)
627 2461-2466.

628 [16] X.L. Warnet, M. Laadhari, A.A. Arnold, I. Marcotte, D.E. Warschawski, A ^2H magic-angle
629 spinning solid-state NMR characterisation of lipid membranes in intact bacteria, *Biochimica et
630 Biophysica Acta (BBA)-Biomembranes*, 1858 (2016) 146-152.

631 [17] P.M. Macdonald, B.D. Sykes, R.N. McElhaney, Fluorine-19 nuclear magnetic resonance
632 studies of lipid fatty acyl chain order and dynamics in *Acholeplasma laidlawii* B membranes. A

633 direct comparison of the effects of cis-and trans-cyclopropane ring and double-bond substituents
634 on orientational order, *Biochemistry*, 24 (1985) 4651-4659.

635 [18] B. McDonough, P.M. Macdonald, B.D. Sykes, R.N. McElhaney, Fluorine-19 nuclear
636 magnetic resonance studies of lipid fatty acyl chain order and dynamics in *Acholeplasma*
637 *laidlawii* B membranes. A physical, biochemical, and biological evaluation of
638 monofluoropalmitic acids as membrane probes, *Biochemistry*, 22 (1983) 5097-5103.

639 [19] M. Gent, P.F. Cottam, C. Ho, Fluorine-19 nuclear magnetic resonance studies of
640 *Escherichia coli* membranes, *Proceedings of the National Academy of Sciences*, 75 (1978) 630-
641 634.

642 [20] M. Gent, P. Cottam, C. Ho, A biophysical study of protein-lipid interactions in membranes
643 of *Escherichia coli*. Fluoromyristic acid as a probe, *Biophysical Journal*, 33 (1981) 211-223.

644 [21] K. Potvin-Fournier, G. Valois-Paillard, M.-C. Gagnon, T. Lefèvre, P. Audet, L. Cantin, J.-F.
645 Paquin, C. Salesse, M. Auger, Novel approaches to probe the binding of recoverin to
646 membranes, *European Biophysics Journal*, 47 (2018) 679-691.

647 [22] M.-C. Gagnon, E. Strandberg, A.S. Ulrich, J.-F. Paquin, M. Auger, New insights into the
648 influence of monofluorination on dimyristoylphosphatidylcholine membrane properties: A solid-
649 state NMR study, *Biochimica et Biophysica Acta (BBA)-Biomembranes*, 1860 (2018) 654-663.

650 [23] K. Koch, S. Afonin, M. Ieronimo, M. Berditsch, A.S. Ulrich, Solid-state ^{19}F -NMR of
651 peptides in native membranes, *Solid state NMR*, (2012) 89-118.

652 [24] E. Strandberg, P. Wadhvani, P. Tremouilhac, U.H. Dürr, A.S. Ulrich, Solid-state NMR
653 analysis of the PGLa peptide orientation in DMPC bilayers: structural fidelity of ^2H -labels versus
654 high sensitivity of ^{19}F -NMR, *Biophysical journal*, 90 (2006) 1676-1686.

655 [25] O.M. Michurin, S. Afonin, M. Berditsch, C.G. Daniliuc, A.S. Ulrich, I.V. Komarov, D.S.
656 Radchenko, Delivering Structural Information on the Polar Face of Membrane-Active Peptides:
657 ^{19}F -NMR Labels with a Cationic Side Chain, *Angewandte Chemie*, 128 (2016) 14815-14819.

658 [26] M. Drouin, P. Wadhvani, S.L. Grage, J. Bürck, J. Reichert, S. Tremblay, M.S. Mayer, C.
659 Diel, A. Staub, J.F. Paquin, Monofluoroalkene-Isostere as a ^{19}F NMR Label for the Peptide
660 Backbone: Synthesis and Evaluation in Membrane-Bound PGLa and (KIGAKI)₃, *Chemistry–A*
661 *European Journal*, 26 (2020) 1511-1517.

662 [27] P.M. Macdonald, B.D. Sykes, R.N. McElhaney, Fluorine-19 nmr studies of lipid fatty acyl
663 chain order and dynamics in *Acholeplasma laidlawii* B membranes. fluorine-19 nmr line shape
664 and orientational order in the gel state, *Biochemistry*, 23 (1984) 4496-4502.

665 [28] M.-C. Gagnon, B. Turgeon, J.-D. Savoie, J.-F. Parent, M. Auger, J.-F. Paquin, Evaluation of
666 the effect of fluorination on the property of monofluorinated dimyristoylphosphatidylcholines,
667 *Organic & Biomolecular Chemistry*, 12 (2014) 5126-5135.

668 [29] M.-C. Gagnon, M. Auger, J.-F. Paquin, Progress in the synthesis of fluorinated
669 phosphatidylcholines for biological applications, *Organic & Biomolecular Chemistry*, 16 (2018)
670 4925-4941.

671 [30] M.-C. Gagnon, P. Ouellet, M. Auger, J.-F. Paquin, Towards the use of monofluorinated
672 dimyristoylphosphatidylcholines as ¹⁹F NMR reporters in bacterial model membranes, *Journal of*
673 *Fluorine Chemistry*, 206 (2018) 43-47.

674 [31] J. Guimond-Tremblay, M.-C. Gagnon, J.-A. Pineault-Maltais, V. Turcotte, M. Auger, J.-F.
675 Paquin, Synthesis and properties of monofluorinated dimyristoylphosphatidylcholine derivatives:
676 Potential fluorinated probes for the study of membrane topology, *Organic & Biomolecular*
677 *Chemistry*, 10 (2012) 1145-1148.

678 [32] D.E. Warschawski, A.A. Arnold, I. Marcotte, A new method of assessing lipid mixtures by
679 ³¹P magic-angle spinning NMR, *Biophysical journal*, 114 (2018) 1368-1376.

680 [33] F. Laydevant, M. Mahabadi, P. Llido, J.-P. Bourgoquin, L. Caron, A.A. Arnold, I. Marcotte,
681 D.E. Warschawski, Growth-phase dependence of bacterial membrane lipid profile and labeling
682 for in-cell solid-state NMR applications, *Biochimica et Biophysica Acta (BBA)-Biomembranes*,
683 1864 (2022) 183819.

684 [34] V. Booth, D.E. Warschawski, N.P. Santisteban, M. Laadhari, I. Marcotte, Recent progress
685 on the application of ²H solid-state NMR to probe the interaction of antimicrobial peptides with
686 intact bacteria, *Biochimica et Biophysica Acta (BBA)-Proteins and Proteomics*, 1865 (2017)
687 1500-1511.

688 [35] T.R. Molugu, S. Lee, M.F. Brown, Concepts and methods of solid-state NMR spectroscopy
689 applied to biomembranes, *Chemical reviews*, 117 (2017) 12087-12132.

690 [36] B. Maraviglia, J.H. Davis, M. Bloom, J. Westerman, K.W. Wirtz, Human erythrocyte
691 membranes are fluid down to - 5 °C, *Biochimica et Biophysica Acta (BBA)-Biomembranes*, 686
692 (1982) 137-140.

693 [37] A.J. Fulco, Fatty acid metabolism in bacteria, *Progress in Lipid Research*, 22 (1983) 133-
694 160.

695 [38] M. Ibarguren, D.J. López, P.V. Escribá, The effect of natural and synthetic fatty acids on
696 membrane structure, microdomain organization, cellular functions and human health, *Biochimica
697 et Biophysica Acta (BBA)-Biomembranes*, 1838 (2014) 1518-1528.

698 [39] R. Koynova, B. Tenchovl, P. Quinn, P. Laggner, Structure and phase behavior of hydrated
699 mixtures of L-dipalmitoylphosphatidylcholine and palmitic acid. Correlations between structural
700 rearrangements, specific volume changes and endothermic events, *Chemistry and physics of
701 lipids*, 48 (1988) 205-214.

702 [40] M.E. Allen, Y. Elani, N.J. Brooks, J.M. Seddon, The effect of headgroup methylation on
703 polymorphic phase behaviour in hydrated N-methylated phosphoethanolamine: palmitic acid
704 membranes, *Soft Matter*, 17 (2021) 5763-5771.

705 [41] K.P. Pauls, A.L. MacKay, M. Bloom, Deuterium nuclear magnetic resonance study of the
706 effects of palmitic acid on dipalmitoylphosphatidylcholine bilayers, *Biochemistry*, 22 (1983)
707 6101-6109.

708 [42] T. Inoue, S.-i. Yanagihara, Y. Misono, M. Suzuki, Effect of fatty acids on phase behavior of
709 hydrated dipalmitoylphosphatidylcholine bilayer: saturated versus unsaturated fatty acids,
710 *Chemistry and Physics of Lipids*, 109 (2001) 117-133.

711 [43] J.H. Davis, The description of membrane lipid conformation, order and dynamics by ^2H -
712 NMR, *Biochimica et Biophysica Acta (BBA)-Reviews on Biomembranes*, 737 (1983) 117-171.

713 [44] D. Marquardt, F.A. Heberle, T. Miti, B. Eicher, E. London, J. Katsaras, G. Pabst, ^1H NMR
714 shows slow phospholipid flip-flop in gel and fluid bilayers, *Langmuir*, 33 (2017) 3731-3741.

715 [45] D.I. Fernandez, M.-A. Sani, A.J. Miles, B.A. Wallace, F. Separovic, Membrane defects
716 enhance the interaction of antimicrobial peptides, aurein 1.2 versus caerin 1.1, *Biochimica et
717 Biophysica Acta (BBA)-Biomembranes*, 1828 (2013) 1863-1872.

718 [46] P.M. Macdonald, B. McDonough, B.D. Sykes, R.N. McElhaney, Fluorine-19 nuclear
719 magnetic resonance studies of lipid fatty acyl chain order and dynamics in *Acholeplasma
720 laidlawii* B membranes. Effects of methyl-branch substitution and of trans unsaturation upon
721 membrane acyl-chain orientational order, *Biochemistry*, 22 (1983) 5103-5111.

- 722 [47] I. Bera, J.B. Klauda, Molecular simulations of mixed lipid bilayers with sphingomyelin,
723 glycerophospholipids, and cholesterol, *The Journal of Physical Chemistry B*, 121 (2017) 5197-
724 5208.
- 725 [48] T. Wang, S.D. Cady, M. Hong, NMR determination of protein partitioning into membrane
726 domains with different curvatures and application to the influenza M2 peptide, *Biophysical*
727 *journal*, 102 (2012) 787-794.
- 728 [49] Y. Yang, H. Yao, M. Hong, Distinguishing bicontinuous lipid cubic phases from isotropic
729 membrane morphologies using ³¹P solid-state NMR spectroscopy, *The Journal of Physical*
730 *Chemistry B*, 119 (2015) 4993-5001.
- 731 [50] B.E. Smart, Fluorine substituent effects (on bioactivity), *Journal of Fluorine Chemistry*, 109
732 (2001) 3-11.
- 733 [51] J.C. Biffinger, H.W. Kim, S.G. DiMugno, The polar hydrophobicity of fluorinated
734 compounds, *ChemBioChem*, 5 (2004) 622-627.
- 735 [52] M. Laadhari, A.A. Arnold, A.E. Gravel, F. Separovic, I. Marcotte, Interaction of the
736 antimicrobial peptides caerin 1.1 and aurein 1.2 with intact bacteria by ²H solid-state NMR,
737 *Biochimica et Biophysica Acta (BBA)-Biomembranes*, 1858 (2016) 2959-2964.

738